INSIGHTS INTO LUNAR MICROSCALE TOPOGRAPHY: EVALUATING PHOTOGRAMMETRY TECHNIQUES USING THE *LUNAR VERTEX* ROVER MULTISPECTRAL MICROSCOPE. Frédéric Diotte[1] (Frederic.Diotte@usherbrooke.ca), Myriam Lemelin[1], Rachel L. Klima[2], Edward A. Cloutis[3] and David T. Blewett[2], [1]Université de Sherbrooke, Sherbrooke, Canada, [2]The Johns Hopkins Applied Physics Laboratory, Laurel, Maryland, U.S.A, [3]University of Winnipeg, Winnipeg, Canada.

Introduction: Topography is commonly evaluated by calculating roughness, a statistical metric that quantifies surface variations. On the Moon, processes such as impact cratering and volcanic flooding generate distinctive multi-scale roughness signatures, detectable through orbital techniques at resolutions coarser than > 1 m [1,2,3,4]. While global roughness maps assist in delineating surface features on larger scales, there is a lack of data for studying topography at smaller scales. The only dedicated instrument that has been used to characterize topography at sub-meter scale is the Apollo Lunar Surface Closeup Camera (ALSCC), a device that acquired stereo-pair imagery with a pixel size of 85 μm, during Apollo 11, 12 and 14. Data acquired by ALSCC revealed variable roughness at the submillimeter to decimeter scale in distinct regions on the Lunar surface, and verified a decrease in surface roughness with scale for these locations [5]. Notable variations in roughness at similar resolutions may also exist in areas like lunar swirls [6] and permanently shadowed regions [7].

Photometric roughness is a key input into the established Hapke model to accurately approximate soil reflectance [8], suggesting small scale topography may influence reflectance measurements acquired by orbital instruments (e.g., LOLA [9] and LAMP [7]). However, the relationship between textural parameters (grain size, roughness, porosity) and the scales dominating reflectance remain ambiguous [10]. Measuring roughness across a broader range of scales would provide insights into the geological processes shaping regions of interest and allow for better calibration of remote sensing data for geological characterization.

Key focus: The deployment of cameras on upcoming lunar rovers will provide means to analyze topography at the micrometer scale in unexplored lunar regions, however many of these payloads are not specifically designed for stereoscopic surface analysis. Here we explore the applicability of different methods for characterizing lunar topography at the submillimeter scale using unstructured imagery, i.e., without a dedicated acquisition plan. We apply the COLMAP photogrammetry pipeline to multi-view images acquired by the *Lunar Vertex* Rover Multispectral Microscope (RMM) engineering model to produce digital elevation models of two regolith simulant samples. We then analyze roughness by calculating the Allan variance, enabling us to compare the multiscale behavior of the topography of the two sample surfaces.

The Rover Multispectral Microscope (RMM): The RMM [11] is a camera paired with an LED illumination board that is part of the *Lunar Vertex* investigation [12], an instrumental suite and rover to be deployed as part of the CLPS CP-11 mission. *Lunar Vertex* will explore the Reiner Gamma lunar swirl and magnetic anomaly located in Oceanus Procellarum (4). RMM consists of a CMOS detector array of 3000×4000 pixels, with a 12mm f/4 lens providing a pixel size of 30 μm for a surface located 20 cm from the camera. RMM will enable a study of the small-scale texture of the soil beneath the rover, as well as the reflectance at 365, 740, 850, 910, and 940 nm.

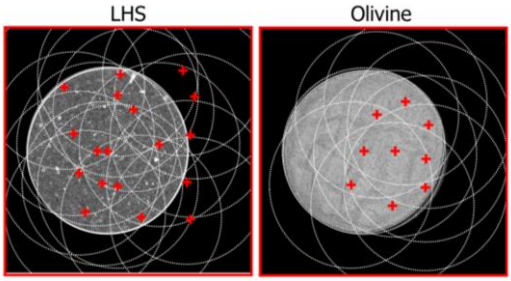

Figure 1. One image is displayed for each sample, overlaid with the centers and perimeters of the sample cup moved in different configurations.

Samples and data: We captured multi-view images at 740 nm of two fine dust samples with different albedos and textures using the RMM engineering model at JHU-APL. The two samples included the Lunar Highlands Simulant (LHS) (Exolith Lab, CLASS), a regolith simulant that we subsequently sieved to retain only grains larger than 300 μm, and olivine dust from the Lunar Constituent Mineral Samples (Exolith Lab, CLASS), with 99 % of grains finer than 110 μm. Our approach to multi-view image acquisition is to move the sample around in the camera's fixed field of view (Fig. 1), enabling the topography of the samples to be captured from different perspectives. 18 images were obtained with the LHS sample, and 9 images were acquired with the olivine sample. The area surrounding the sample cups was masked out to prevent the photogrammetry algorithm from matching spatially invariant targets.

3D reconstruction: We use the COLMAP Structure-from-Motion and Multi-view Stereo pipeline

[13,14] to perform a 3D reconstruction of the samples' surfaces using multi-view images as inputs. Structure-from-motion (SfM) is a projective geometry-based approach for creating 3D representations using multiple images captured at different angles of the same surface. The 3D reconstructions were aligned to a common coordinate system using the coordinates of a selected feature for each sample and a 20 cm elevation value. Meshes were generated using a screened Poisson surface reconstruction and projected onto a 1700×1700 pixel grid using linear interpolation. A local tilt correction is also performed by removing a least-squares plane from the digital elevation model.

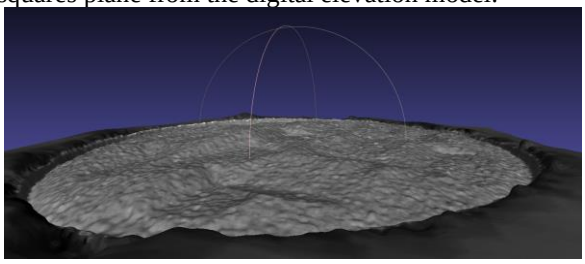

Figure 2. The resulting mesh for the olivine sample visualized in MeshLab.

Roughness analysis: Following [5], we calculate the mean Allan variance (Eq. 1) as an indicator of roughness for different scales Δx, where z is the elevation and the mean is obtained for all horizontal positions, x_j. Variances are calculated up to 10% of the length of the topographic profile and are then visualized through a variogram.

$$\bar{v}_A^2 = \frac{1}{N}\sum_{j=1}^{N}\left[z(x_j + \Delta x) - z(x_j)\right]^2 \quad (1)$$

The Allan variance is also related to the Hurst exponent for fractal surfaces through Eq. 2, with $0 > H > 1$, where $H = 1$ describes self-similarity, indicating that roughness is replicated at all scales.

$$\bar{v}_A^2 = v_{ref}^2 \Delta x^{2H} \quad (2)$$

Results: The elevation maps (Fig. 3) allow to assess the different textures of the two samples. The topography of the LHS is dominated by the high-frequency pattern of grains and by the mound at the center of the sample cup, while the olivine dust is characterized by a smoother surface with the texture formed by the spatula becoming apparent on a larger scale. The sieved LHS sample has a higher Allan variance at all scales and is therefore rougher than the olivine dust sample (Fig. 4). LHS and olivine have respective Hurst exponents of 0.94 and 0.95 for the interval 30 - 300 µm, indicating near self-similar behavior at these scales. Both surfaces are multilinear, with a break towards a lower slope at a baseline of around 300 µm. The break is more pronounced for LHS than for olivine, meaning that the sample surface becomes smooth more rapidly with scale.

This experiment demonstrates that the approach used can differentiate soils with different grain size distributions.

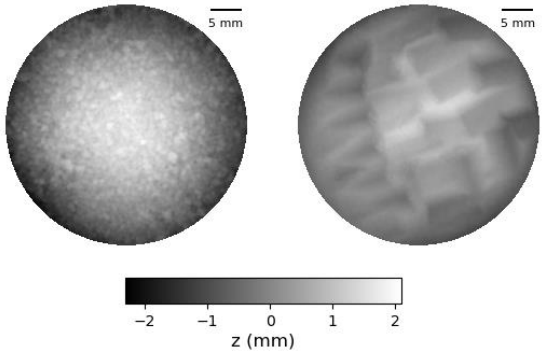

Figure 3. Detrended digital surface models show elevations ranging from -2.3 to 2.1 mm for LHS, and from -1.4 to 1.5 mm for olivine.

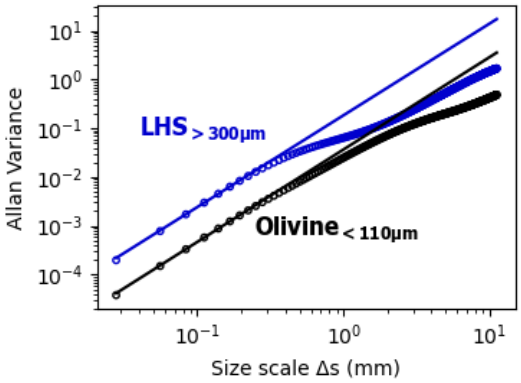

Figure 4. Allan variograms for 30 µm < Δx < 3 mm. The straight lines are the best fit of the power law from Eq. 2 to the variograms at the small scales.

Acknowledgements: This project was undertaken with the financial support of the Canada Research Chair in Northern and Planetary Geological Remote Sensing, NSERC, and the Canadian Space Agency grant [22EXPVIPER] held by Prof. Lemelin.

References: [1] Cao *et al.* (2015), *PSS, v. 108*, 13 – 23. [2] Kreslavsky *et al.* (2013), *Icarus, v. 226(1)*, 52 – 66. [3] Lemelin *et al.* (2020), *JGR Planets*, 125, e2019JE006105. [4] Rosenburg *et al.* (2011), *JGR Planets, v. 116, E02001*. [5] Helfenstein and Shepard (1999), *Icarus*, 141, 107. [6] Garrick-Bethell *et al.* (2011), *Icarus, vol. 212*(2), 480-492. [7] Gladstone *et al.* (2012), *JGR Planets, v. 117*, E00H04. [8] Hapke, B. (2012) *Camb. Univ. Press, Theory of Refl. and Emitt. Spect*., 2nd ed. [9] Lucey *et al.* (2014), *JGR Planets, v. 119(7)*, 1665-1679. [10] Schiltz and Bachmann (2023), *Icarus, v. 390*, 115240. [11] Klima *et al.* (2023), *LPSC 54th*, abstract #2718. [12] Blewett *et al.* (2023*), LPSC 54th*, abstract #1780. [13] Schönberger *et al.* (2016), CVPR 2016, ISSN 1063-6919. [14] Schönberger *et al.* (2016), ECCV 2016, 501-518.